Catal Lett (2007) 119:148–153
DOI 10.1007/s10562-007-9212-8

# Enhanced Photocatalytic Hydrogen Evolution Over $CaTi_{1-x}Zr_xO_3$ Composites Synthesized by Polymerized Complex Method

**Wei Sun · Shuqing Zhang · Cheng Wang · Zhixiang Liu · Zongqing Mao**

Received: 5 June 2007 / Accepted: 9 July 2007 / Published online: 25 July 2007


**Abstract** The solid solution of $CaTi_{1-x}Zr_xO_3$ ($x$ = 0–0.15) was successfully synthesized by the polymerized complex (PC) method. This study has exhibited the advantage of the PC method to prepare a highly active $CaTiO_3$ compared with the conventional solid-state reaction (SSR) method. More importantly, further improvement in phase purity and large surface area was achieved by the doping of $Zr^{4+}$, leading to remarkable enhancement of photocatalytic activities compared to pure $CaTiO_3$. The quantum yield for $H_2$ evolution over the most active photocatalyst, Pt (1.0 wt%)/$CaTi_{0.93}Zr_{0.07}O_3$, was 1.91% and 13.3% in photoreactions from pure water and aqueous ethanol solution, respectively for 0.1 g photocatalyst, which was about 3.3 and 2.5 times compared to that of PC-derived $CaTiO_3$.

**Keywords** $CaTi_{1-x}Zr_xO_3$ · Polymerized complex method · Photocatalytic activity · Hydrogen evolution

## 1 Introduction

Perovskite-type oxide materials based on transition metals with d(0) electron configuration such as Ti(IV), Nb(V) and Ta(V) have been investigated as efficient photocatalysts for photodecomposition of water under UV irradiations [1–7]. $CaTiO_3$ is one of the alkaline earth titanates with perovskite structure such as $SrTiO_3$ and $BaTiO_3$. These titanates have various attractive properties from the electrical and optical viewpoints. The crystal structure of $CaTiO_3$ is, strictly speaking, $GdFeO_3$ type derived from distorting the ideal cubic perovskite structure [8]. It is known that the $BaTi_4O_9$ compound of pentagonal-prism tunnel structure, though bringing about a significantly large distortion of $TiO_6$ octahedra, exhibits much higher activities in photocatalytic H2 production than the ideal perovskite of $BaTiO_3$ [9, 10]. Therefore, the investigation concerning the photocatalytic activity of $CaTiO_3$ is important as well as other alkaline earth titanates. The studies on photocatalytic $H_2$ evolution of $CaTiO_3$ were limited in literatures [11, 12], and new preparation methods or modifications aiming at high surface area and phase purities were needed for the enhancement of photoactivities.

The Pechini-type polymerized complex (PC) method is based on the chelation of metal cations by a hydroxycarboxylic acid. It has a great advantage over the conventional solid-state reaction method in that a phase-pure compound can be prepared at reduced temperatures for a shorter reaction time, especially in terms of mixing of elements at a molecular lever [13–17]. In this study, the feasibility of the PC route for the synthesis of calcium titantes was conducted. On the other hand, the influences of $Zr^{4+}$ doping to $CaTiO_3$ on phase stability, optical properties and the photocatalytic performance were investigated. A highly improved photoactivity for $H_2$ evolution over Pt/$CaTi_{0.93}Zr_{0.07}O_3$ photocatalyst was reported.

## 2 Experimental

All chemicals were of analytical grade and used without further purification. Powders of $CaTi_{1-x}Zr_xO_3$ with $x$ = 0,

W. Sun · C. Wang · Z. Liu · Z. Mao (✉)
Institute of Nuclear and New Energy Technology,
Tsinghua University, Beijing 100084, PR China
e-mail: maozq@tsinghua.edu.cn

S. Zhang
College of Material Science and Chemistry Engineering,
China University of Geosciences, Wuhan 430074, PR China

0.01, 0.03, 0.05, 0.07, 0.10, and 0.15 were synthesized by the polymerized complex method (PCM). $Ti(OC_4H_9)_4$ (TBOT), $Ca(NO_3)_2$, $ZrO(Cl_2) \cdot 8H_2O$ was selected as starting materials. An amount of 0.02 mol of TBOT was first dissolved into 0.8 mol of ethylene glycol (EG), and subsequently 0.16 mol of citric acid (CA) was added to this solution. After complete dissolution, a solution containing 0.02 mol of $Ca(NO_3)_2$ and the selected doping amount of $ZrO(Cl_2) \cdot 8H_2O$ was added in dropwise. The resulted transparent solution was stirred at 50 °C for 2 h. Then it was heated at 140–150 °C for several hours with continuous stirring to accelerate polyesterification, resulted in a highly viscous gel without any visible precipitation. The precursor of black powder was achieved by charring the gel at 350 °C for 2 h in an electric furnace. $CaTi_{1-x}Zr_xO_3$ was finally synthesized by calcining the precursor at 900 °C for 2 h. For comparison, non-doped $CaTiO_3$ was also prepared by the conventional solid-state reaction method (SSRM); a stoichiometric mixture of $CaCO_3$ and $TiO_2$ (P25, Degussa) was ground mechanically and then calcined at 1,100 °C for 10 h. Pt cocatalysts (1.0 wt%) was loaded from an aqueous $H_2PtCl_6 \cdot 6H_2O$ solution by a photodeposition method.

The crystal structures of prepared catalysts were characterized by X-ray diffraction (XRD, D/Max-RB, Cu Kα). The surface area was determined by the Brunauer–Emmett–Teller method using nitrogen gas as absorbent (BET, NOVA 4000). The morphology of single crystals was observed by transmission electron microscopy (TEM, JEOL JEM-200CX). The diffuse reflectance UV–vis absorption spectra were collected on a UV–vis spectrometer (DRS, Hitachi U-3010). The photoluminescence emission spectra were recorded by a fluorescence spectrophotometer (PL, Perkin-Elmer LS55) with an excitation wavelength of 300 nm at room temperature.

Photocatalytic reactions for $H_2$ evolution were carried out in a gas-closed circulation system. The photocatalyst powder (0.1 g) was dispersed in deionized water (100 ml) or aqueous ethanol solution (100 ml of deionized water, 20 ml of $C_2H_5OH$) by means of magnetic stirring in a 390 ml reaction cell made of quartz glass. A 500 W high-pressure Hg lamp was used as the light source and irradiated from the top of the cell. To avoid the heating of the solution during illuminations, cool water was circulated through a quartz jacket around the wall of cell. The reaction temperature was constantly adjusted to 30 ± 2 °C. The amount of evolved $H_2$ was determined by gas chromatography (Shimazu GC-14B; TDX-01 column, TCD, Ar carrier) through a gas sampler (0.5 ml) which was directly connected to the reaction system. The quantum yield is the more meaningful parameter than the rate of $H_2$ evolution itself to gauge the performance of a photocatalyst because the rate is normalized against the absorbed photons [1]. The apparent quantum yield was determined as below.

Quantum yield = [(2 × the amount of evolved $H_2$)/the number of incident photons]×100%

The number of incident photons was calculated by the chemical actinometer of potassium ferrioxalate ($K_3Fe(C_2O_4)_3 \cdot 3H_2O$), which was estimated to be $4.07 \times 10^{-6}$ mol $s^{-1}$. In this case, it is considered that the 365 nm emission of the high-pressure Hg lamp is the major promoter of the reaction.

## 3 Results and Discussion

Figure 1a shows the XRD patterns of $CaTi_{1-x}Zr_xO_3$ ($x$ = 0–0.15) powders synthesized by PCM and SSRM. All the samples showed major phase of orthorhombic perovskite structure in good agreement with the diffraction pattern of $CaTiO_3$ (JCPDF 42-0423). In the sample prepared by SSRM at 1,150 °C for 10 h, the three strongest lines of rutile $TiO_2$ were identified, which was due to impurities resulting from the difficulty in interdiffusion of the precursors during calcinations. For the PC sample of $CaTiO_3$, though a peak around 29.35° was observed as impurity which might be due to nonstoichiometric byproduct of calcium titanates, no phases of CaO or $TiO_2$ appeared as

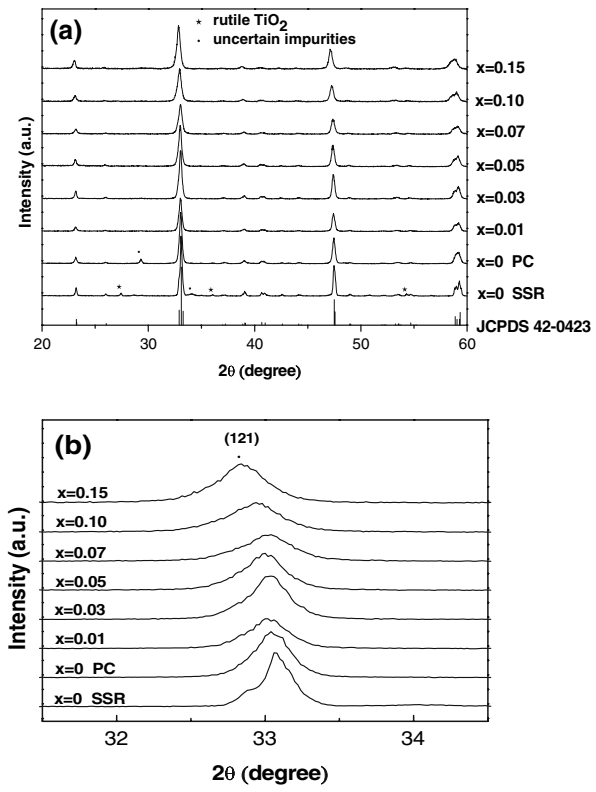


**Fig. 1** (**a**) XRD patterns of $CaTiO_3$ prepared by SSRM at 1,100 °C for 10 h and $CaTi_{1-x}Zr_xO_3$ ($x$ = 0–0.15) prepared by PCM at 900 °C for 2 h; (**b**) enlargement of the region around 33° ($2\theta$)

distinct impurities, implying an improved homogeneity in the PC-derived gel precursors.

Both materials of $CaTiO_3$ and $CaZrO_3$ have orthorhombic perovskite structures with similar lattice parameters ($CaTiO_3$: $a = 5.4424$, $b = 7.6417$, $c = 5.3807$. $CaZrO_3$: $a = 5.7558$, $b = 8.0101$, $c = 5.5929$), indicating that different composition of $CaTi_{1-x}Zr_xO_3$ can constitute a solid solution of $CaTiO_3$ and $CaZrO_3$ in limited ranges of doping content. As in Fig. 1a, unlike pure $CaTiO_3$, all the $Zr^{4+}$ doped samples of different compositions ($x = 0.01$–$0.15$) showed single-phase nature without the identification of impurity or new phases of zirconia. It suggested that the solid solution of $CaTi(Zr)O_3$ compounds can stabilize the ionic bonding between Ca and octahedron $Ti(Zr)O_6$, preventing the crystallization of dissociated impurities and unstoichiometric byproducts. For $CaTi_{1-x}Zr_xO_3$, the $Ti^{4+}$ sites of the bulk center are partially substituted by $Zr^{4+}$. Since the ionic radius of $Zr^{4+}$ (0.79 Å) is bigger than that of $Ti^{4+}$ (0.68Å), the unit cell will be enlarged and cause slight changes in crystal parameters. As in Fig. 1b, the broadened diffraction peaks and gradual shifting of the (121) diffraction peak to lower angles can confirm the deformation fact of $Zr^{4+}$ introduction.

Table 1 summarizes the average crystallite size estimated from XRD patterns using the Sherrer formula and the BET surface area of all samples. In general, the calculated crystal sizes of $CaTi_{1-x}Zr_xO_3$ showed distinct decreases with increasing $Zr^{4+}$ content, indicating that the doping of $Zr^{4+}$ can suppress the grain growth and lead to smaller grain size, which was in consistent with the results in literatures [18, 19]. Another important characteristic of the $CaTi_{1-x}Zr_xO_3$ powders prepared by PCM is their relatively large surface areas when compared with the SSR sample. In addition, the surface area showed a dramatic increase with increasing $Zr^{4+}$ content to 7 mol% and then a quick drop when increasing to 15 mol% of $Zr^{4+}$ substitute. It is known that having a crystalline material with a larger surface area is of practical importance for certain application, particularly a catalytic application [3]. It can be anticipated that the solid solution of $CaTi(Zr)O_3$ with appropriate $Zr^{4+}$ content with high surface areas would exhibit higher catalytic activities than pure $CaTiO_3$.

TEM image of $CaTiO_3$ prepared by SSRM, $CaTiO_3$ and Pt loaded $CaTi_{0.93}Zr_{0.07}O_3$ prepared by PCM is shown in Fig. 2. A distinct decrease in the particle size of the PC-derived $CaTiO_3$ is observed compared to the SSR sample, in which the SSR sample exhibits much larger particle size than the crystalline size estimated in Table 1, implying the large particle size of SSR sample is already beyond the application range of Sherrer's equation. It is evident for the size controlling effect of doped $Zr^{4+}$ to pure $CaTiO_3$ when comparing Fig. 2b and c. The $CaTi_{0.93}Zr_{0.07}O_3$ sample exhibited relatively uniform morphology with average particle size of approximately 32 nm in good accordance with the crystallite size estimated from XRD, indicating that each grain can be considered as a single crystallite. Moreover, a few dark spots can be seen from the image, representing high electron density, and they correspond to the deposition of dispersive Pt species with particle size of 2–3 nm.

The diffuse reflection spectra of $CaTiO_3$ prepared by SSRM and $CaTi_{1-x}Zr_xO_3$ powders of different compositions ($x = 0$, 0.03, 0.07, 0.15) prepared by PCM are shown in Fig. 3. The value of the band gaps for all samples were shown in Table 1, which was determined from the energy intercept by extrapolations of the straight regions of the absorption coefficient $(\alpha h\nu)^2$ versus h$\nu$ for a direct allowed transition [18]. For the SSR sample, a shoulder peak at a wavelength of about 380 nm is probably associated with the delocalized electronic levels introduced by crystal defects [20]. In addition, both of the SSR and PC sample of pure $CaTiO_3$ exhibit relatively higher absorption in the visible range, which should also be an evidence for the absorption of impurities. By doping $Zr^{4+}$, the value of band gap is found to become slightly larger than that of pure $CaTiO_3$. This may result of the wider band gap of $ZrO_2$ (~5.50 eV) compared with that of $CaTiO_3$ (~3.55 eV), and the overall band gap of the $CaTi(Zr)O_3$ solid solution can be thought to depend on the degree of Ti 3d and Zr 4d orbitals being involved in the conduction band.

**Table 1** Physical properties evaluated from XRD patterns, BET method and DRS of the $CaTi_{1-x}Zr_xO_3$ photocatalysts

| $x$ in $CaTi_{1-x}Zr_xO_3$ | Synthesis method | Position of d (121) ($2\theta$/degree) | Crystallite size[a] (nm) | BET surface area ($m^2\ g^{-1}$) | Band gap[b] (eV) |
|---|---|---|---|---|---|
| 0 | SSR | 33.07 | 68.3 | 5.29 | 3.550 |
| 0 | PC | 33.05 | 58.5 | 8.23 | 3.567 |
| 0.01 | PC | 33.02 | 51.2 | 10.68 | 3.571 |
| 0.03 | PC | 33.02 | 45.5 | 16.16 | 3.572 |
| 0.05 | PC | 32.97 | 34.1 | 25.75 | 3.598 |
| 0.07 | PC | 33.00 | 29.3 | 29.07 | 3.592 |
| 0.10 | PC | 32.94 | 24.1 | 28.37 | 3.599 |
| 0.15 | PC | 32.84 | 34.1 | 10.66 | 3.622 |

[a] Estimated from line broadening of d (121) diffraction peak using Sherrer formula

[b] Calculated from the straight regions of the absorption coefficient $(\alpha h\nu)^2$ versus $h\nu$ near the band edge

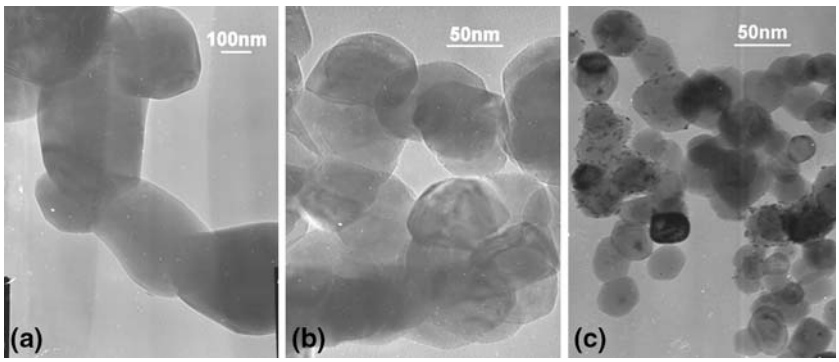


**Fig. 2** TEM images of (**a**) $CaTiO_3$ prepared by SSRM, (**b**) $CaTiO_3$ and (**c**) Pt (1.0 wt%)/ $CaTi_{0.93}Zr_{0.07}O_3$ prepared by PCM

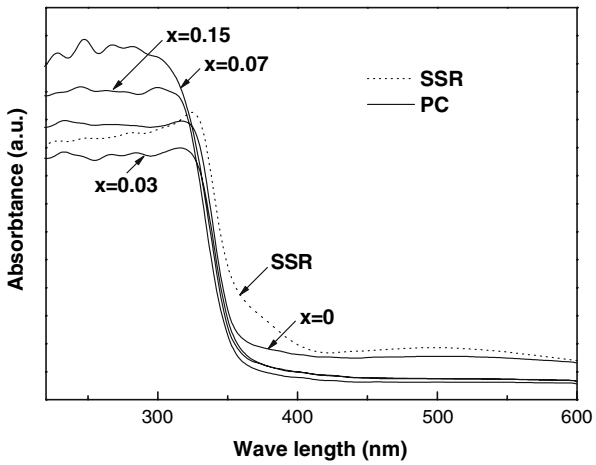


**Fig. 3** Diffuse reflectance spectra of $CaTiO_3$ prepared by SSRM and $CaTi_{1-x}Zr_xO_3$ powders of different compositions ($x$ = 0, 0.03, 0.07, 0.15) prepared by PCM

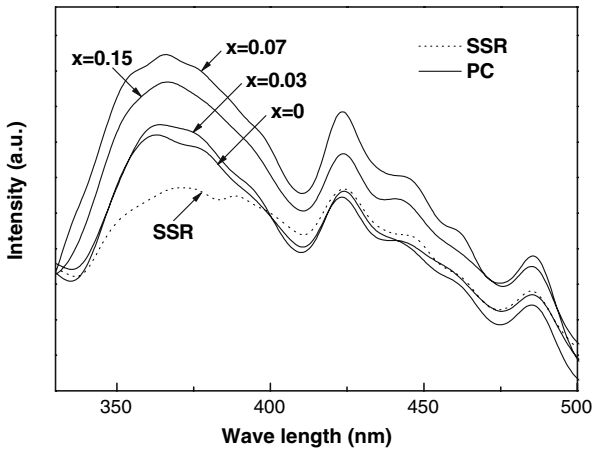


**Fig. 4** Room-temperature PL spectra ($\lambda_{ex}$ = 300 nm) of $CaTiO_3$ prepared by SSRM and $CaTi_{1-x}Zr_xO_3$ powders of different compositions ($x$ = 0, 0.03, 0.07, 0.15) prepared by PCM

The photoluminescence emission spectra have been widely used to investigate the efficiency of charge carrier trapping, immigration and transfer, and to understand the fate of electron/hole pairs in semiconductor particles [21]. Figure 4 shows the PL emission spectra with an excitation wavelength of 300 nm at room temperature. All the samples exhibit in approximately the same shape. The main emission peak at about 366 nm was attributed to a direct recombination of a conduction electron in Ti 3d orbital and a hole in O 2p valence band. The difference between the bandgap energy (~3.55 eV) and the emission peak energy (~3.39 eV), which is around 0.16 eV, is described as the Stokes shift due to the Frank–Condon effect [22]. The blue band at about 423 nm and a green band at about 485 nm can be associated with the radiative recombination process of self-trapped excitons or hydroxylated $Ti^{3+}$ surface complexs located in the forbidden gap [23]. It was found that the PL intensity of the PC-derived $CaTiO_3$ was greatly increased compared with the SSR sample, and the increase in intensity went on with the doping of $Zr^{4+}$ up to 7 mol%. The variation in PL intensity may result from the change of defect state on the surface [24]. The smaller the grain size, the greater the number of the d-surface states and thus of the localized sensitizing centers, so that the recombination via self-trapped excitons is enhanced. Finally, the emission band increases in intensity with decreasing grain size. In addition, impurities in bulk can enhance non-radiative recombination of the excited electrons, leading to decrease in emission intensity [22], which could also explain the low PL intensity of the SSR sample.

In photocatalytic experiments, the loading of reduced Pt was quite effective for $CaTiO_3$ to promote hydrogen production, but the formation of $O_2$ was not detected during photodecomposition of water. It has been concerned that catalyst may be deactivated by accumulations of a peroxidized phase. Therefore, catalysts which form a stoichiometric amount of $O_2$ are required from a long-term stability point of view [25]. $NiO_x$ was reported to be an efficient cocatalyst for overall water splitting into $H_2$ and $O_2$, but it was found to be ineffective for $H_2$ evolution over $CaTi(Zr)O_3$. Further study on effective modifications of $CaTiO_3$ for overall water splitting is under investigations. In this article, the modification of Pt loading was focused. Figure 5 shows typical time courses of $H_2$ evolution from

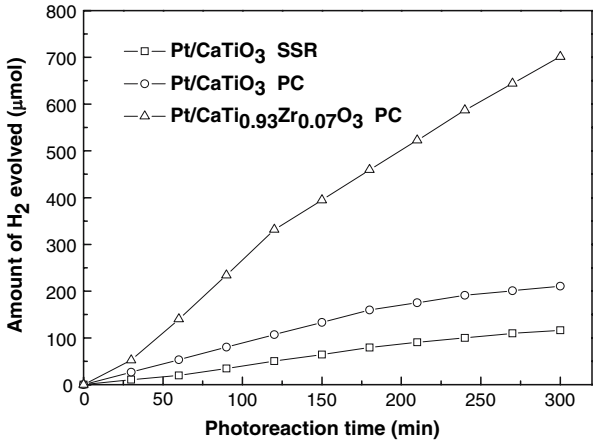


**Fig. 5** Time courses of $H_2$ evolution from pure water over (□) Pt/$CaTiO_3$ prepared by SSRM, (○) Pt/$CaTiO_3$ and (Δ) Pt/$CaTi_{0.93}Zr_{0.07}O_3$ prepared by PCM. Reaction conditions: Pt loading 1 wt%; catalyst 0.1 g; deionized water 100 ml; Outer irradiation of 500 W high-pressure Hg lamp from the top of the cell made of quartz

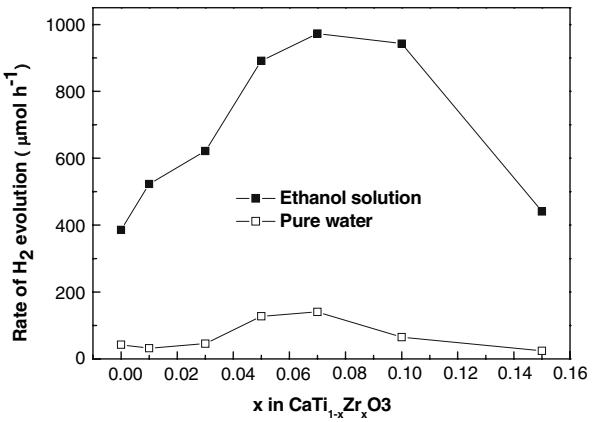


**Fig. 6** Effects of composition $x$ on the photocatalytic $H_2$ evolution from pure water (100 ml) or aqueous ethanol solution (100 ml of deionized water, 20 ml of $C_2H_5OH$) over Pt/$CaTi_{1-x}Zr_xO_3$ synthesized by PCM ($x$ = 0–0.15)

photodecomposition of water over Pt-loaded SSR and PC samples. It is clear that, compared to SSRM, the PC method has the advantage of obtaining higher photocatalytic activities with large surface area and low lattice defects. The $CaTiO_3$ prepared by PCM produced nearly twice amount of $H_2$ compared to the SSR sample. Another inspiring fact is that with the doping of $Zr^{4+}$ up to 7 mol%, the photocatalytic hydrogen production reached a rate of 140 μmol $h^{-1}$, about 3.3 times compared to that of PC-derived $CaTiO_3$. As discussed above, the improvement in crystal integrity, suppression in grain growth and increase in surface area were caused by the doping of $Zr^{4+}$. It favors faster arrival of photoexcited electrons from bulk to surface reactive sites and reduces the amounts of recombination centers for photogenerated electron-hole pairs [26], which greatly enhanced the photocatalytic activities.

In overall water splitting, oxidation of water by holes is a slower process than reduction by electrons. In order to facilitate the oxidation, hole-scavengers are often introduced. An additional 20 ml of ethanol was applied here to obtain improved $H_2$ evolution. Figure 6 shows the dependence of $Zr^{4+}$ content on the rate of $H_2$ evolution from pure water and aqueous ethanol solution. The remarkable increase of photoactivity was achieved in ethanol solution. Both of the two lines showed that the photoactivity was greatly enhanced with the increase of $Zr^{4+}$ content up to 7 mol%, and then decreased to the level close to undoped $CaTiO_3$ when $Zr^{4+}$ content was increased to 15 mol%. The quantum yield for $H_2$ evolution over the most active photocatalyst, Pt/$CaTi_{0.93}Zr_{0.07}O_3$, was 1.91% and 13.3% in photoreactions from pure water and aqueous ethanol solution, respectively for 0.1 g photocatalyst. The changes in photoactivity for Pt/ $CaTi_{1-x}Zr_xO_3$ can be best explained by the terms of surface area, which exhibits the same trend in accordance with the rates of evolved H2. In addition, appropriate amounts of $Zr^{4+}$ have good effects on improved crystal perfection, which may also accounts for the rapid increase in photoactivities. However, with the doping of excessive $Zr^{4+}$ content, the solid solution of $CaTi(Zr)O_3$ turned to be unstable for overlarge deformations introduced by $Zr^{4+}$, the lattice distortion of crystal structure by excessive $Zr^{4+}$ substitutions may act as recombination centers [3], leading to a dramatic drop on the photocatalytic acitivity when $Zr^{4+}$ content was over 10 mol%.

In order to investigate the stability of the PC-derived sample under photocatalytic conditions, the crystal structure of $CaTi_{0.93}Zr_{0.07}O_3$ was studied before and after photoreactions. The XRD pattern of $CaTi_{0.93}Zr_{0.07}O_3$ before the reaction was identical to that measured after a prolonged photoreaction for 10 h (in Fig. 7), suggesting that the catalyst is stable under UV light and in the aqueous medium.

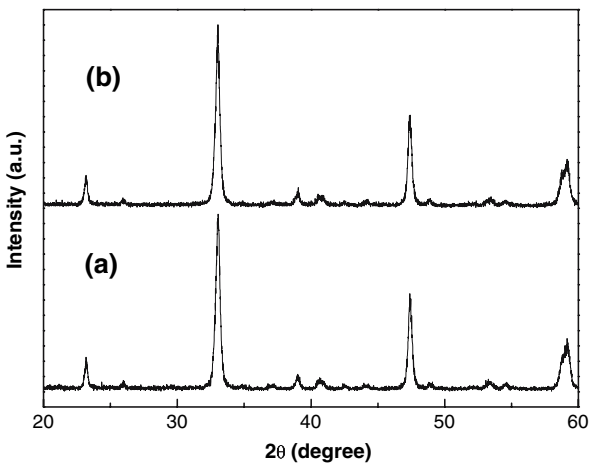


**Fig. 7** XRD patterns of Pt(1.0 wt%)/$CaTi_{0.93}Zr_{0.07}O_3$ (**a**) before, and (**b**) after photoreaction of 10 h irradiation

## 4 Conclusions

In summary, the solid solution of $CaTi_{1-x}Zr_xO_3$ ($x$ = 0–0.15) was successfully synthesized by the PC method at 900 °C for 2 h. Compared to the traditional SSR method, the advantage of PC method to prepare a crystallite material of improved homogeneity with high surface area resulted in enhanced photoactivity in photodecomposition of water. Moreover, It revealed that doping of a appropriate amount of $Zr^{4+}$ (5–7 mol%) was highly effective for increasing the activity of photocatalytic $H_2$ evolution over $Pt/CaTiO_3$ catalyst. The results showed good respondence with the improvement in crystal integrity, suppression in grain growth and increase in surface area caused by $Zr^{4+}$ substitutions. Consequently, this study exhibited that the doping of $Zr^{4+}$ to subsitiute appropriate amounts of $Ti^{4+}$ would be an efficient way to promote photocatalytic activities.

**Acknowledgments** The work was financially supported by the National Basic Research Program of China (973 Program) (No. 2003 CB214500), National High Technology Research and Development Program of China (863 Program) (No. 2006AA03Z223), Specialized Research Fund for the Doctoral Program of Higher Education of China (No. 20030003069) and "Solar Hydrogen" Project sponsored by Shell Hydrogen.

## References

1. Hwang DW, Kim HG, Kim J, Cha KY, Kim YG, Lee JS (2000) J Catal 193:40
2. Thaminimulla CTK, Takata T, Hara M, Kondo JN, Domen K (2000) J Catal 196:362
3. Yoshino M, Kakihana M (2002) Chem Mater 14:3369
4. Kato H, Asakura K, Kudo A (2003) J Am Chem Soc 125:3082
5. Zou Z, Yin J, Ye JH (2003) J Phys Chem B 107:61
6. Yoshioka K, Petrykin V, Kakihana M, Kato H, Kudo A (2005) J Catal 232:102
7. Abe R, Higashi M, Sayama K, Abe Y, Sugihara H (2006) J Phys Chem B 110:2219
8. Ueda K, Yanagi H, Noshiro R, Hosono H, Kawazoe H (1998) J Phys-Condens Mat 10:3669
9. Kakihana M, Arima M, Sato T, Yoshida K, Yamashita Y, Yashima M, Yoshimura M (1996) Appl Phys Lett 69:2053
10. Yamashita Y, Tada M, Kakihana M, Osada M, Yoshida K (2002) J Mater Chem 12:1782
11. Mizoguchi H, Ueda K, Orita M, Moon S-C, Kajihara K, Hirano M, Hosono H (2002) Mater Res Bull 37:2401
12. Wang GY, Wang YJ, Zhao XQ, Zhang HT (2005) Chin J Catal 26:138
13. Ikeda S, Hara M, Kondo JN, Domen K, Takahashi H, Okubo T, Kakihana M (1998) Chem Mater 10:72
14. Ko YG, Lee WY (2002) Catal Lett 83:157
15. Kim HG, Hwang DW, Bae SW, Jung JH, Lee JS (2003) Catal Lett 91:193
16. Hwang DW, Kirn HG, Lee JS, Kim J, Li W, Oh SH (2005) J Phys Chem B 109:2093
17. Jeong H, Kim T, Kim D, Kim K (2006) Int J Hydrogen Energ 31:1142
18. Hirano M, Nakahara C, Ota K, Tanaike O, Inagaki M (2003) J Solid State Chem 170:39
19. Wang YM, Liu SW, Lu MK, Wang SF, Gu F, Gai XZ, Cui XP, Pan J (2004) J Mol Catal a-Chem 215:137
20. Pontes FM, Pinheiro CD, Longo E, Leite ER, de Lazaro SR, Varela JA, Pizani PS, Boschi TM, Lanciotti F (2003) Mater Chem Phys 78:227
21. Yamashita H, Ichihashi Y, Zhang SG, Matsumura Y, Souma Y, Tatsumi T, Anpo M (1997) Appl Surf Sci 121:305
22. Rahman MM, Krishna KM, Soga T, Jimbo T, Umeno M (1999) J Phys Chem Solids 60:201
23. Li XZ, Li FB, Yang CL, Ge WK (2001) J Photochem Photobiol A 141:209
24. Meng JF, Huang YB, Zhang WF, Du ZL, Zhu ZQ, Zou GT (1995) Phys Lett A 205:72
25. Tatsumi Ishihara HN, Fukamachi K, Takita Y (1999) J Phys Chem B 103:1
26. Jing DW, Zhang YJ, Guo LJ (2005) Chem Phys Lett 415:74